Published in final edited form as:

Cell Rep. 2021 July 13; 36(2): 109345. doi:10.1016/j.celrep.2021.109345.

SIRT4 is an early regulator of branched-chain amino acid catabolism that promotes adipogenesis

Elma Zaganjor[1,3,*], **Haejin Yoon**[1], **Jessica B. Spinelli**[1], **Elizabeth R. Nunn**[3], **Gaëlle Laurent**[1], **Paulina Keskinidis**[1], **Suganja Sivaloganathan**[1], **Shakchhi Joshi**[1], **Giulia Notarangelo**[1], **Stacy Mulei**[1], **Mathew T. Chvasta**[3], **Sarah A. Tucker**[1], **Krystle Kalafut**[1], **Robert A.H. van de Ven**[1], **Clary B. Clish**[2], **Marcia C. Haigis**[1,4,*]

[1]Department of Cell Biology, Blavatnik Institute, Harvard Medical School, Boston, MA 02115, USA

[2]Broad Institute of MIT and Harvard, Cambridge, MA 02142, USA

[3]Department of Molecular Physiology and Biophysics, Vanderbilt University, Nashville, TN 37232, USA

[4]Lead contact

SUMMARY

Upon nutrient stimulation, pre-adipocytes undergo differentiation to transform into mature adipocytes capable of storing nutrients as fat. We profiled cellular metabolite consumption to identify early metabolic drivers of adipocyte differentiation. We find that adipocyte differentiation raises the uptake and consumption of numerous amino acids. In particular, branched-chain amino acid (BCAA) catabolism precedes and promotes peroxisome proliferator-activated receptor gamma (PPARγ), a key regulator of adipogenesis. In early adipogenesis, the mitochondrial sirtuin SIRT4 elevates BCAA catabolism through the activation of methylcrotonyl-coenzyme A (CoA) carboxylase (MCCC). MCCC supports leucine oxidation by catalyzing the carboxylation of 3-methylcrotonyl-CoA to 3-methylglutaconyl-CoA. Sirtuin 4 (SIRT4) expression is decreased in adipose tissue of numerous diabetic mouse models, and its expression is most correlated with BCAA enzymes, suggesting a potential role for SIRT4 in adipose pathology through the alteration of BCAA metabolism. In summary, this work provides a temporal analysis of adipocyte differentiation and uncovers early metabolic events that stimulate transcriptional reprogramming.

Graphical abstract

*Correspondence: elma.zaganjor@vanderbilt.edu (E.Z.), marcia_haigis@hms.harvard.edu (M.C.H.).

AUTHOR CONTRIBUTIONS

E.Z. and M.C.H. conceived the study, designed experiments, wrote the paper, and analyzed data. E.Z., J.B.S., S.J., and C.B.C. performed and analyzed mass spectrometry experiments. E.Z., H.Y., and G.L. conducted *in vivo* mouse experiments. E.Z., H.Y., E.R.N., P.K., S.S., S.M., G.L., G.N., S.A.T., K.K., and R.A.H.d.V. performed experiments on gene expression, protein levels, and microscopy. E.Z. and M.T.C. performed bioinformatics analysis.

SUPPLEMENTAL INFORMATION

Supplemental information can be found online at https://doi.org/10.1016/j.celrep.2021.109345.

DECLARATION OF INTERESTS

The authors declare no competing interests.

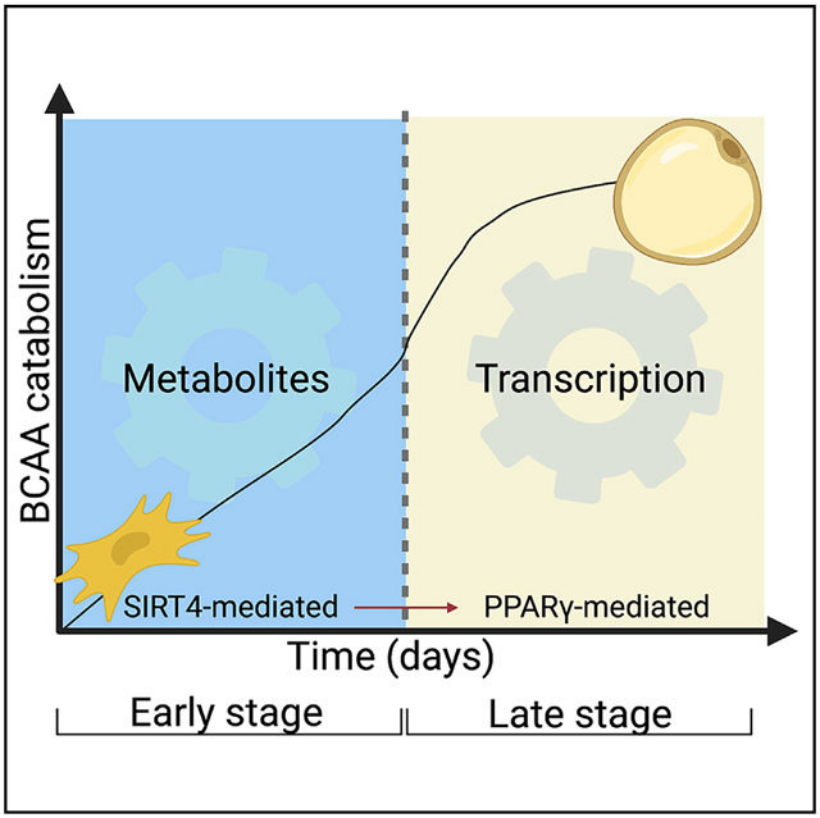

In brief

Although adipose tissue expands and shrinks in response to nutrients, the involvement of mitochondrial signaling in adipose tissue biology has remained elusive. Zaganjor et al. identify an early regulator of adipogenesis, a mitochondrial sirtuin, SIRT4, which promotes the process through the induction of branched-chain amino acid catabolism.

INTRODUCTION

Obesity, a pandemic associated with an increased risk of death and accelerated aging, is a major cause of insulin resistance and type 2 diabetes (T2D). Dysregulation of lipid metabolism caused by obesity underlies T2D pathology. The initial stages of weight gain promote healthy adipose tissue expansion and differentiation, a process known as adipogenesis. Adipogenesis is thought to be a protective mechanism that allows for excess nutrients to be stored as fat, rather than to be released into the bloodstream where they can drive insulin resistance and lipotoxicity in peripheral tissues. Thus, elucidating the mechanism of adipose tissue expansion is critical for our understanding of the etiology of insulin resistance and T2D.

The transcriptional program that mediates adipogenesis is well characterized. This process is mediated by transcriptional master regulators CCAAT/enhancer binding proteins (C/EBPs) and peroxisome proliferator-activator receptor gamma (PPARγ) (Gregoire et al., 1998). C/EBPα and PPARγ support differentiation by activating adipose-tissue-specific gene

expression and by enhancing each other's expression (Rosen, 2005). Furthermore, this positive feedback between C/EBPα and PPARγ also modulates the expression of genes involved in insulin sensitivity, connecting adipocyte differentiation to protective mechanisms against the pathophysiology of T2D (Wu et al., 1999).

Although the temporal aspect of the transcriptional control of adipogenesis has been studied in detail (Rosen, 2005), our understanding of the early metabolic changes during adipogenesis is incomplete. To gain a broad view of the metabolic rewiring that occurs during initiation of differentiation, we profiled 176 metabolites in cell culture media and in 3T3-L1 cells 2 days after differentiation was induced. Branched-chain amino acids (BCAAs) were the most consumed metabolites in differentiating adipocytes. Interestingly, mature adipocytes have been shown to use BCAAs for acetyl-coenzyme A (CoA) production for lipogenesis (Green et al., 2016). However, whether BCAAs play a role in the initiation of adipogenesis in early stages and subsequently contribute to the onset of adipose-tissue-mediated insulin resistance is unclear. To probe the fate of BCAAs in early adipogenesis, we used stable isotope tracing of leucine and determined that leucine is oxidized, generating NADH for the electron transport chain (ETC). This early metabolic event precedes PPARγ, a hallmark of adipogenesis. Mechanistically, we determined that the mitochondrial sirtuin 4 (SIRT4) promotes early BCAA catabolism by increasing the activity of methylcrotonyl-CoA carboxylase (MCCC). However, at later stages of adipogenesis, PPARγ boosts BCAA catabolism, consistent with the published literature (Blanchard et al., 2018). In summary, the temporal regulation of BCAA catabolism during adipogenesis appears to be bimodal, involving early post-translational and late transcriptional mechanisms. Importantly, we find that SIRT4 promotes PPARγ activity and adipocyte differentiation *in vitro*. *In vivo*, adipose-tissue-specific SIRT4-knockout (AKO) mice have higher BCAA levels in gonadal white adipose and an increased ratio of BCAAs to their catabolic intermediates in the plasma, consistent with decreased BCAA catabolism. Thus, we have identified SIRT4 as a key player in the regulation of BCAA catabolism in the adipose tissue that controls an early program of adipocyte differentiation.

RESULTS

BCAA catabolism is induced in early adipogenesis

Fuel switching has been observed in adipogenesis (Trefely and Wellen, 2018). We postulated that early metabolic changes may be drivers of adipogenesis rather than a consequence of altered cellular state. To study how metabolism is altered in adipogenesis, we used 3T3-L1 cells, a well-established pre-adipocyte cell model whose differentiation into adipocytes can be induced by a cocktail containing 3-isobutyl-1-methylxanthine (IBMX), dexamethasone, and insulin. Because at day 2 of differentiation 3T3-L1 cells have not yet accumulated lipid droplets as assessed by BODIPY and oil red O staining (Figures S1A and S1B), we chose this time point to evaluate early metabolic events in adipocyte differentiation. Using mass spectrometry, we identified which metabolites are differentially exchanged (taken up and secreted) in undifferentiated versus differentiating (2 day) cells (Figure 1A). Using MetaboAnalyst 4.0, we noted that amino acid metabolic pathways were the top signatures that were altered in early adipogenesis (Figure S1C). Particularly, BCAAs (leucine,

isoleucine, and valine), as well as amino acids that are commonly co-imported with BCAAs (tyrosine, tryptophan, and phenylalanine), were preferentially taken up in differentiating adipocytes (Figures 1A, S1C, and S1D). Urea cycle and polyamine biosynthesis metabolites (ornithine and putrescine) were the most secreted metabolites, which could be indicative of increased detoxification of NH_3 generated by amino acid catabolism (Figures 1A and S1D).

The possibility that amino acids are taken up and catabolized by differentiating adipocytes prompted us to measure intracellular metabolites. We isolated metabolites from adipocytes by using a 6-day differentiation time course and assessing metabolite levels every 2 days (Figure S1E). As expected, we found increased accumulation of numerous lipid species, such as acylcarnitines and lysophospholipids, with advanced differentiation (Figure S1E). This is consistent with adipocyte function of storing fats. Conversely, intracellular amino acids were most depleted during early differentiation, signifying increased consumption (Figures S1E and S1F). These results indicate profound reprogramming of metabolite use during early adipocyte differentiation.

Because circulating BCAA levels are an important marker of diabetic state and BCAAs were both significantly taken up and depleted from differentiating adipocytes (Figures 1B and 1C), we aimed to further investigate the temporal aspect of BCAA use in adipogenesis. To directly test whether BCAA catabolism is altered during adipogenesis, we performed stable isotope tracing of leucine by using [U-$^{13}C_6$]leucine and assessing its incorporation into downstream metabolites throughout 3T3-L1 differentiation (Figure 1D). We detected increasing levels of ^{13}C incorporation into the TCA cycle intermediate α-ketoglutarate, indicating enhanced leucine oxidation. This oxidation persisted into later stages of adipogenesis as well, along with subsequent increased incorporation of ^{13}C label in glutamate and glutamine (Figure 1D). Acetyl-CoA produced by leucine catabolism can contribute to lipogenesis or enter the TCA cycle to generate NADH for use in the ETC for ATP production. We evaluated the possibility that oxidized leucine contributes to mitochondrial respiration using α-ketoisocaproic acid, a metabolic intermediate of leucine catabolism, as a sole substrate and measured oxygen consumption rate (OCR) after 1 and 2 days of adipogenesis initiation (Figure S1G). We observed elevated OCR when comparing early adipogenic cells to undifferentiated 3T3-L1 adipocytes (Figure S1G).

Given that differentiating adipocytes favor amino acid uptake and consumption, we tested if supplying an excess of BCAAs is sufficient to enhance adipogenesis. Using oil red O as a read out of adipogenesis, we found that the addition of 10 mM leucine, isoleucine, and valine promotes adipogenesis (Figure S1H). Complimentarily, we performed differentiation for 8 days in media lacking leucine and evaluated the expression of differentiation markers compared to cells cultured in leucine-rich media. In the absence of leucine, we noted decreased expression of transcription factor PPARγ and its targets perilipin and FABP4, highlighting the requirement of leucine for adipogenesis (Figure 1E). Under these conditions, we did not detect changes in proliferation and growth signaling pathway mTORC1, as assessed by no change in the phosphorylation of ribosomal protein S6 (Figure S1I). As leucine is oxidized and contributes carbon to tricarboxylic acid (TCA) cycle intermediates, we postulated that supplementation of TCA cycle intermediates in the absence of leucine could rescue the differentiation defect. Indeed, adding back cell-

permeable dimethyl-α-ketoglutarate rescued differentiation in the absence of leucine (Figure 1E). To examine the possibility that the adipogenic cocktail can induce changes in BCAA metabolism even in the absence of differentiation, we examined the non-adipogenic NIH/3T3 cells. Addition of the differentiation cocktail to NIH/3T3 cells did not alter the intracellular BCAAs leucine, isoleucine, or valine, suggesting that these changes are associated with adipogenesis (Figure S1J). Overall, our data point to an early dependency on BCAA catabolism for adipocyte differentiation.

BCCA catabolism during early adipogenesis is not dependent on PPARγ

The BCAA catabolic pathway is catalyzed by a number of key enzymes including branched-chain keto acid dehydrogenase E1, alpha subunit (BCKDHA), branched-chain keto acid dehydrogenase E1, beta subunit (BCKDHB), and methylcrotonyl-CoA carboxylase 1 (MCCC1) (Figure 2A). We observed increased levels of these enzymes after 2 days of adipogenesis, and their elevated expression persisted through later stages of differentiation, consistent with increased BCAA catabolism (Figure 2B). Notably, the mRNA expression of many of these enzymes was substantially induced only after 4 days of differentiation, suggesting that the induction of BCAA catabolism predates the transcriptional regulation of the associated enzymes (Figures 2C and S2A). Previous studies identified PPARγ as a major inducer of BCAA levels in the blood (Blanchard et al., 2018). Therefore, we temporally dissected the relationship between PPARγ activity and BCAA catabolism. To assess the requirement of PPARγ for BCAA catabolism in early adipogenesis, we measured the mRNA expression of key enzymes in leucine catabolism in the presence or absence of the PPARγ orthosteric inhibitor T0070907 (Figures 2D and S2B). We found that the canonical PPARγ target *Adipoq* (adiponectin) was induced as early as day 1 of adipogenesis, and this event was blocked completely by PPARγ inhibition, demonstrating on-target activity of the inhibitor in our cell system (Figure 2D). Conversely, the mRNA levels of BCAA catabolic enzymes were less increased and sometimes even decreased at day 1 of adipogenesis, and thus, PPARγ had less of an effect on the induction of these enzymes (Figures 2D and S2B). SR16832, a more potent inhibitor of PPARγ, showed a stronger demand of PPARγ for sustained mRNA expression of *Pcca* and *Bckdhb* (Figure S2C). However, protein levels of BCAA catabolic enzymes were unaffected by PPARγ inhibition after 1 day of differentiation by either inhibitor (Figures 2E and S2D). Alternatively, 6 days of inhibition of PPARγ led to suppression of the BCAA catabolic enzymes BCKDHA and MCCC1 and differentiation markers FABP4 and perilipin (Figure 2F). These data suggest the requirement of PPARγ activity for sustained BCAA enzyme expression. Given that pharmacological inhibitors could induce changes by off-target effects, we used a genetic approach, stably knocking down PPARγ with two distinct short hairpin RNAs (shRNAs) (Figure S2F). Loss of PPARγ had little to no effect on the expression of BCAA catabolic genes in early differentiation, but PPARγ was required for sustained expression of these enzymes (Figures S2F–S2H).

Next, to examine the functional necessity of intact PPARγ activity on BCAA catabolism, we performed leucine tracing in the presence or absence of PPARγ inhibition after 1 day of adipogenesis. We detected increased ^{13}C labeling of TCA cycle intermediates after 1 day of adipogenesis as compared to the undifferentiated state, indicating that leucine catabolism is

increased in early adipogenesis (Figures 2G and S2E). However, pharmacological inhibition of PPARγ had no effect on leucine contribution to α-ketoglutarate or glutamate at this early stage of adipogenesis (Figures 2G and S2E). Thus, BCAA catabolism in early adipogenesis is not dependent upon PPARγ transcriptional activity.

Because BCAA catabolism remains induced even at later stages of adipogenesis, we evaluated the influence of PPARγ on BCAA catabolism at these advanced stages of differentiation. After prolonged inhibition of PPARγ in the later stage of adipogenesis, we noted suppression of leucine catabolism, as demonstrated by decreased ^{13}C incorporation into α-ketoglutarate or glutamate (Figure 2G). This finding is consistent with published observations that PPARγ stimulates BCAA catabolism (Blanchard et al., 2018). Thus, prolonged PPARγ inhibition may blunt BCAA catabolism by downregulating adipogenesis itself.

SIRT4 promotes adipogenesis and PPARγ

Given that BCAA catabolism is a mitochondrial process, we explored the involvement of SIRT3, SIRT4, and SIRT5, which are NAD^+-dependent deacylases and key regulators of mitochondrial metabolic enzymes (Giblin et al., 2014; van de Ven et al., 2017). These sirtuins were induced upon adipocyte differentiation, with the largest increase in SIRT4 expression (Figures 3A and S3A). To interrogate the role of mitochondrial sirtuins in 3T3-L1 differentiation, we overexpressed SIRT3, SIRT4, and SIRT5. SIRT4 overexpression caused the greatest increase in adipogenesis, as assessed by oil red O staining (Figures 3B and S3B–S3D). In contrast, SIRT3 had no effect on adipogenesis, and SIRT5 only modestly increased adipogenesis. To examine if SIRT4 is necessary for adipogenesis, we used 2 different shRNAs to knockdown SIRT4 (shSIRT4) and a scrambled shRNA control (shControl) in 3T3-L1 cells (Figure S3E). We found that the loss of SIRT4 impaired adipocyte differentiation (Figure 3C). To determine if SIRT4 catalytic activity is indispensable for its function in adipogenesis, we overexpressed SIRT4 wild type (WT) and a catalytically inactive SIRT4 H162Y mutant (SIRT4HY) (Figure S3F). Overexpression of SIRT4HY did not increase oil red O accumulation, indicating that adipogenesis requires SIRT4 catalytic activity (Figures 3D and S3F).

As adipocyte differentiation induces a well-characterized transcriptional program that further promotes lipid accumulation, we tested whether SIRT4 expression alters adipogenesis by modulating this transcriptional program. Indeed, SIRT4 overexpression enhanced expression of the adipogenic factors *CEBPa*, *Cidea*, *Acsl1*, and *PPARγ* (Figure 3E). Furthermore, SIRT4 knockdown cells displayed downregulation of the transcriptional profile that stimulates adipogenesis (Figure S3G). Next, we monitored the expression of PPARγ in a time course of differentiation. Cells overexpressing SIRT4 have increased levels of PPARγ, whereas SIRT4 knockdown cells had lower levels of PPARγ than control cells (Figures 3F and S3H). Importantly, pharmacological inhibition of PPARγ fully inhibited differentiation (assessed by suppression of perilipin) but had no effect on the induction of SIRT4 expression at 2 days of differentiation (Figures 3G and 3H). Taken together, these data demonstrate that SIRT4 induction predates PPARγ activation during adipocyte differentiation.

SIRT4 promotes BCAA catabolism

In *Caenorhabditis elegans*, SIRT4 interacts with biotin-dependent carboxylases, which include the BCAA catabolic enzyme MCCC1 (Wirth et al., 2013). Moreover, a proteomics study in fibroblasts showed that SIRT4 binds various enzymes in BCAA catabolism (Mathias et al., 2014). Anderson et al., (2017) demonstrated that SIRT4 elevates MCCC1 activity, and SIRT4 deficiency is associated with hyperacylation of MCCC1 in the liver. Given the established connection between SIRT4 and BCAA enzymes, we hypothesized that SIRT4 may boost adipogenesis by the regulation of BCAA catabolism (Figure 4A). To test this hypothesis, we profiled metabolites in SIRT4-overexpressing and knockdown 3T3-L1 adipocytes to evaluate whether SIRT4 affects BCAA levels. Analysis of metabolic profiles of WT and SIRT4-overexpressing cells differentiated for 2 days identified BCAA metabolism and aminoacyl tRNA biosynthesis as the two pathways further induced by SIRT4 (Figure S4A). Valine and isoleucine uptake were increased in SIRT4-overexpressing adipocytes both in their undifferentiated state and after 2 and 6 days of differentiation (Figures S4B and S4C), and leucine uptake was similarly increased by SIRT4 overexpression at 2 and 6 days after differentiation (Figure 4B). To determine whether BCAA catabolism is increased by SIRT4 overexpression, we monitored intracellular valine, isoleucine, and leucine levels. Similar to control cells, differentiation causes intracellular BCAA depletion in SIRT4-overexpressing cells (Figures 4C, S4D, and S4E). Because SIRT4-overexpressing cells have a higher uptake but relatively similar intracellular amounts of BCAAs, we postulated that SIRT4 induces BCAA catabolism. To directly measure if SIRT4 is required to alter the rate of BCAA catabolism, we used control and shRNA-mediated SIRT4 knockdown. Tracing with [U-$^{13}C_6$]leucine, incorporation of the label into α-ketoglutarate and glutamate was diminished in shSIRT4 cells, indicating that SIRT4 elevates leucine catabolism during adipocyte differentiation (Figure 4D). To establish whether the loss of SIRT4 prevents BCAA catabolism from supporting respiration, we examined α-ketoisocaproic-acid-mediated OCR. We demonstrated that loss of SIRT4 leads to decreased OCR early in differentiation, thus revealing that SIRT4 promotes leucine catabolism to drive mitochondrial respiration (Figure 4E).

To explore whether leucine catabolism is required for adipogenesis, we used a genetic approach and knocked down MCCC1, which catalyzes the carboxylation of 3-methylcrotonyl-CoA to 3-methylglutaconyl-CoA (Figure S4F). Loss of MCCC1 resulted in reduced mitochondrial respiration using α-ketoisocaproic acid as a substrate, without any change in glucose-dependent respiration (Figures 4F and S4G). Importantly, adipogenesis was decreased in MCCC1 knockdown cells, illustrating that BCAA catabolism is a driver of adipogenesis (Figure 4G). Considering that previous studies showed that SIRT4 promotes MCCC1 activity in the liver, we examined if MCCC1 activity is altered in early adipogenesis. We performed an *in vitro* MCCC1 activity assay based on production of [^{14}C] 3-methylglutaconyl-CoA from [^{14}C]bicarbonate and 3-methylcrotonyl-CoA. To test for specificity of the assay, we used shControl and shMCCC1 knockdown cells. As expected, knockdown of MCCC1 significantly lessened the signal in this assay (Figure S4H). Next, we compared undifferentiated and 1- or 2-day differentiated 3T3-L1 cells and uncovered increased MCCC1 activity after 1 day of differentiation, a time point at which MCCC1

protein expression is not induced (Figures S4I and S4J). Altogether, these data exposed early activation of MCCC1 and its requirement for adipogenesis.

To determine if MCCC1 activity during early differentiation is dependent on SIRT4, we performed the activity assay at day 2 of differentiation in shControl and shSIRT4 3T3-L1 cells. SIRT4 knockdown significantly blunted MCCC1 activity, suggesting that SIRT4 regulates BCCA catabolism through MCCC1 (Figure 4H). Under these conditions, SIRT4 knockdown did not affect MCCC1 mRNA or protein levels (Figures S4K and S4L). In line with the observation that PPARγ had no effect on BCAA catabolism during early differentiation, we also observed no effect of PPARγ inhibition on MCCC1 activity (Figure S4N). To examine if MCCC1 activity in differentiating 3T3-L1 adipocytes is modulated by methylglutaryl modification as reported in the liver, we immunoprecipitated MCCC1 and measured this acylation by western blotting. We detected no methylglutarylation on MCCC1 under these conditions (Figure S4M). Our findings suggest that SIRT4 elevates MCCC1 activity in adipocytes as in the liver, although the precise mechanism of this regulation may be distinct. To interrogate if MCCC1 is required for SIRT4-mediated adipogenesis, we knocked down MCCC1 in the context of SIRT4 overexpression (Figure S4O). We find that MCCC1 knockdown suppresses SIRT4-mediated increase in perilipin and FABP4, suggesting that SIRT4 promotes adipogenesis through MCCC1 (Figure 4I).

Loss of SIRT4 in the adipose tissue in vivo results in decreased BCAA catabolism

Our *in vitro* studies revealed that SIRT4 mediates BCAA catabolism in differentiating adipocytes. To examine if SIRT4 promotes BCAA catabolism in adipose tissue *in vivo*, we generated a SIRT4 Flox mouse strain and crossed it with AdipoqCre mice to knockout SIRT4 in the adipose (AKO) specifically (Figures 5A and 5B). We first profiled metabolic characteristics of this new strain by comparing the weight gain of control Flox mice and AKO mice on a standard chow diet and noted no difference over a period of 12 weeks (Figure S5A). Similarly, the mice had comparable food intake and a small difference in fat body composition (Figures 5C and S5B). Whole-body indirect calorimetry showed that the respiratory exchange ratio (RER) was comparable between control and AKO mice (Figure S5D). We found no difference in activity between Flox and AKO mice at 22°C or 4°C by using infra-red (IR) beams (Figure S5C). We observed no obvious morphological differences between the adipose of Flox and AKO mice fed a standard chow diet (Figure 5D).

Because SIRT4 promotes BCAA catabolism in our cellular model, we interrogated whether the loss of SIRT4 in adipose tissue has an effect on BCAA levels in this tissue. We detected elevated valine, while leucine and isoleucine trended up without reaching statistical significance in gonadal white adipose tissue of AKO mice (Figure 5E). The increased BCAAs in gonadal adipose tissue in AKO mice were indicative of reduced BCAA catabolism.

Tissue-specific alterations in BCAA oxidation result in systemic changes in levels of BCAAs and their catabolic intermediates (Neinast et al., 2019). To determine if the loss of SIRT4 in the adipose tissue had an effect on systemic BCAA oxidation, we analyzed plasma metabolites by mass spectrometry. The AKO mice displayed an accumulation of BCAAs and a trend toward depletion of BCAA catabolic intermediates in the plasma, suggesting that

SIRT4 activity in adipose tissue affects systemic BCAA catabolism (Figures 5F and S5E). Finally, the reduced capacity of AKO mice to catabolize BCAAs was further reflected by the increased ratio of BCCAs to ketoacids in their plasma (Figure 5G).

SIRT4 expression in adipose tissue correlates with BCAA enzyme expression in diabetic models

Our laboratory previously discovered that full-body knockout (KO) mice have no obvious phenotypes in weight gain or insulin tolerance on a standard chow diet (Laurent et al., 2013b). However, on a high-fat diet (HFD) challenge, SIRT4 KO mice are protected from weight gain but are more insulin resistant (Anderson et al., 2017; Laurent et al., 2013b; Zaganjor et al., 2017). BCAA catabolism enzymes are downregulated in the adipose tissue of diabetic patients and mouse models, resulting in plasma accumulation of BCAAs. Given that SIRT4 regulates BCAA catabolism and protects from obesity-mediated phenotypes such as insulin resistance, we hypothesized that SIRT4 may be downregulated in diabetic models (Herman et al., 2010; Pietiläinen et al., 2008). For this purpose, we used a publicly available dataset, the Attie Lab Diabetic Database (Keller et al., 2008). We surveyed expression profiles of T2D mouse model leptin mutants (ob/ob) and normal control mice of two distinct strains, namely, B6 and BTBR, that were 4 or 10 weeks old. After 10 weeks, ob/ob mice were obese and had lower SIRT4 expression in the adipose tissue in both genetic backgrounds (Figure S5G). At 4 weeks, ob/ob mice in the B6 background had lower SIRT4 expression in the adipose tissue (Figure S5G). The effect of HFD on reducing SIRT4 expression was significant in the adipose tissue, but not in other metabolic organs, including the liver or soleus (Figure S5G). The BCAA degradation pathway was a top metabolic pathway correlated with SIRT4 expression, and the top genes that correlated with SIRT4 expression in this pathway were MCCC1, BCKDHA, and BCAT2 (Figures S5H and 5H). SIRT4 expression did not broadly correlate with mitochondrial abundance but rather with specific mitochondrial metabolic pathways, as genes commonly used to assess mitochondrial content, such as VDAC and HSP60, were not consistently decreased in diabetic adipose tissue (Figures S5F and S5H). These data support the hypothesis that SIRT4 and BCAA catabolic enzymes are functionally linked in pathological obesity-driven mouse models.

DISCUSSION

White adipose tissue is a dynamic metabolic organ that governs the storage and release of energy in response to fuel availability. Even though adipocytes differentiate in response to nutrients, little is known about how metabolism drives differentiation. Here, we used a metabolomics approach to identify pathways altered in early adipogenesis. We demonstrate that certain amino acids, and in particular BCAAs, are consumed during early stages of differentiation. BCAA catabolism supports mitochondrial respiration at this stage of adipogenesis. As adipocytes store nutrients in the form of fat, ATP-dependent lipogenesis pathways are highly active. Thus, BCAA-induced mitochondrial respiration in early adipogenesis may facilitate ATP generation for lipogenesis at later stages of the process. At later stages of adipogenesis, BCAA catabolism generates carbon for lipogenesis (Green et al., 2016). These observations point to the importance of mitochondria in white adipose

tissue development. A complementary study by Kusminski et al. (2012) identified changes in adipokine secretion due to alterations in mitochondrial iron metabolism, further giving merit to mitochondria in the context of white adipose tissue function.

Our study highlights a fundamental role of mitochondria as the site of nutrient oxidation that is critical for stimulating a transcriptional program long known to be essential for adipogenesis. Importantly, SIRT4 and induction of BCAA catabolism amplify expression of PPARγ and its targets, which also include BCAA catabolism enzymes. Thus, we have identified an early event in adipose differentiation that uses direct metabolic regulation by small metabolites to propagate a well-defined transcriptional program of adipogenesis through a positive feedforward loop. Such elegant regulation was previously described between glucose metabolism and carbohydrate response element binding protein (ChREBP), linking glucose oxidation and transcription in adipogenesis (Fernandez et al., 2019).

Although it is unclear how SIRT4 function in the mitochondria impacts transcriptional activity of PPARγ, there is a precedent for it. Previous work from our group showed that the loss of SIRT4 increases expression of PPARα target genes in fatty acid catabolism (Laurent et al., 2013a). Mechanistically, in the absence of SIRT4, NAD^+ levels are elevated and activate SIRT1 that can then be recruited to PPARα and co-regulate transcription.

Previous work identified the link between SIRT4 and BCAA catabolism through MCCC1 in the liver (Anderson et al., 2017). Here, we find that SIRT4 also enhances MCCC1 activity in adipocytes and that loss of this regulation results in decreased adipogenesis. SIRT4 has been reported to bind to numerous substrates involved in BCAA catabolism including MCCC1, BCKDHA, dihydrolipoamide branched-chain transacylase (DBT), and dihydrolipoyl dehydrogenase (DLD) (Anderson et al., 2017; Mathias et al., 2014), raising the possibility that SIRT4 engages this pathway at multiple enzymatic nodes. Additional investigation is required to determine which SIRT4-BCAA catabolism enzyme interactions are most important for promoting adipogenesis. Interestingly, under our conditions of adipogenesis, we do not observe the previously reported activity of SIRT4 on MCCC1 as a modulator of lysine methylglutarylation. Given that numerous enzymatic activities of SIRT4 have been revealed (Bheda et al., 2016; Feldman et al., 2012; Zaganjor et al., 2017), it is possible that SIRT4 augments MCCC1 activity in adipocytes through a previously unidentified activity.

Clinically, elevated levels of valine, leucine, isoleucine, tyrosine, and phenylalanine have been measured in the plasma of T2D human subjects and are associated with insulin resistance (Felig et al., 1969; Newgard et al., 2009). How BCAA levels and related metabolites rise in obese and insulin-resistant humans is not well understood, although several possibilities have been proposed, such as increased protein consumption or contribution from the gut microbiome. Furthermore, inhibiting BCAA catabolism in brown adipose tissue advances obesity and glucose intolerance (Yoneshiro et al., 2019). Recent studies using *in vivo* isotopic tracing found that insulin-resistant mice exhibit decreased BCAA catabolism in adipose and liver, causing increased shunting of BCAA oxidation to the muscle and enhanced muscle lipotoxicity (Neinast et al., 2019). In this study, we generated a new adipose-tissue-specific AKO mouse model and demonstrated that SIRT4 expression in mature adipocytes promotes oxidation of BCAAs *in vivo*. In the future, it will

be important to examine if the loss of SIRT4 in pre-adipocytes results in defects in adipogenesis *in vivo* and the effect of this regulation on HFD-induced insulin resistance. In summary, this work defines an early step in adipogenesis regulated by SIRT4-mediated stimulation of BCAA metabolism with important developmental implications in adipocytes.

STAR★METHODS

RESOURCE AVAILABILITY

Lead contact—Further information and requests for resources and reagents should be directed to and will be fulfilled by the Lead Contact, Marcia Haigis (Marcia_Haigis@hms.harvard.edu).

Materials availability—Reagents generated in this study will be made available on request, but we may require a completed Materials Transfer Agreement if there is potential for commercial application.

Data and code availability—This study did not generate any unique datasets or code.

EXPERIMENTAL MODEL AND SUBJECT DETAILS

Cell lines—3T3-L1 cells were cultured in DMEM (Life Technologies) supplemented with 10% FBS (Life Technologies) and 1% penicillin and streptomycin (Invitrogen). 3T3-L1 were induced with a differentiation cocktail containing 1.5 μg/mL insulin, 0.5 mM 3-isobutyl-1-methylxantine (IBMX), 1 μM dexamethasone. The media was changed every 2 days for a differentiation time course. NIH/3T3 cells were cultured in DMEM (Life Technologies) supplemented with 10% FBS (Life Technologies) and 1% penicillin and streptomycin (Invitrogen).

Mice—ES cells containing floxed Sirt4 were purchased at the International Knockout Mouse Consortium (EUCOMM). The ES cells were implanted in receiving mice, which gave birth to 13 chimera mice. These chimera mice were then bred with C57BL/6 mice giving a F1 generation, which were bred together. F2 mice were bred with Flp mice to remove the cassette containing the gene LAcZ and Neo to obtain our final SIRT4 flox strain. SIRT4 flox allele (Flox) mice were crossed with AdipoqCre mice to knockdown SIRT4 specifically in the adipose. Female mice, 20–22 weeks of age were used in our studies. All animals were used in accordance with animal care guidelines from the Harvard Medical School Standing Committee on Animals and the National Institutes of Health. All mouse protocols were approved by the Harvard Medical Area Standing Committee on Animals.

METHOD DETAILS

Immunofluorescence—To stain lipid droplets, cells were incubated with the fluorescent fatty acid BODIPY 558/568 C12 (2 mM; #D3835; ThermoFisher) for 15 minutes at 37°C. Cells were extensively washed and immediately fixed with 4% paraformaldehyde for 20 minutes at RT. Samples were washed and permeabilized using 0.25% Triton X-100 in PBS for 5 minutes at room temperature and afterward blocked with 5% BSA in PBS for 1 hour. Images were collected on an inverted Niko Ti spinning disk confocal equipped with a CSU-

X1 spinning disk (Yokogawa), an ORCA-R2 cooled CCD camera (Hamamatsu), and a Spectral Applied Research LMM-5 laser merge module including a solid-state 488nm (100mW) and 561nm (100mW) lasers. Imaged were acquired with a 405/488/568/647 dichroic and ET525/50 m and ET620/60 m emission filters. Maximum projections were created from z stacks using ImageJ.

Oil Red O staining and quantification—Adipogenesis was quantified by Oil Red O staining using standard protocol. Briefly, post differentiation, cells were washed in PBS, fixed with 3.7% formalin, washed with 60% isopropanol, and then stained with 0.3% Oil Red O solution. Excess stain was removed by washing the cells with sterile water, and cells were then dried for imaging. Finally, lipid droplets were solubilized in 100% isopropanol and quantified by determining the resultant absorbance at 492nm. Cells were counterstained with 0.01% crystal violet and extracted with 100% methanol and absorbance was measured at 570nm. This method was used to assess later stages of adipocyte differentiation.

Generation of stable cell lines—Short hairpin RNAs (shRNAs) against SIRT3, SIRT4, and SIRT5, and MCCC1 were subcloned into the pLKO.1 puro vector (Addgene Plasmid #8453) at EcoRI and AgeI sites. Hairpin oligonucleotides used for subcloning are listed in supporting document Table S2. Subcloning was confirmed with sequencing. Subcloned plasmids were transfected into HEK293T cells with lentiviral packaging vectors. After 48 hours, lentivirus was harvested and target cells were infected in the presence of 8 μg/mL polybrene. Following infection, cells were selected with puromycin.

For overexpression studies, we used plasmids pBabe-HA-SIRT3, pBabe-HA-SIRT4, pBabe-HA-SIRT5. Sequencing reactions were carried out with an ABI3730xl DNA analyzer at the DNA Resource Core of Dana-Farber/Harvard Cancer Center.

Western blots—Adherent cells were washed twice with PBS and lysed with NP40 lysis buffer (1% NP40, 1 mM DTT, 0.2% phosphatase inhibitor cocktail 2 and phosphatase inhibitor cocktail 3 (Sigma), 1 cOmplete protease inhibitor tablet (Sigma)) or RIPA lysis buffer (50 mM HEPES, 150 mM NaCl, 0.1% SDS, 0.5% sodium deoxycholate, 1% Triton X-100, 1 mM DTT, 1 cOmplete protease inhibitor tablet (Sigma), 0.2% phosphatase inhibitor #2 & #3 (Sigma)) for experiments involving mitochondrial proteins. Protein content was quantified using a BCA Assay (Thermo Scientific) and equal protein was run on 10%–20% Tris-HCl Gel (BioRad). Protein was transferred to a nitrocellulose membrane (BioRad). Membranes were incubated with indicated primary antibodies overnight (4°C). Secondary antibodies: AlexaFluor® 546 Goat Anti-Rabbit IgG (H+L), highly cross absorbed (1:10000, Life Tech), Alexa Fluor® 488 Goat Anti-Mouse IgG (H+L) Antibody, highly cross-absorbed (1:10000, Life Tech). Blots were imaged with the Odyssey CLx infrared imaging system (LI-COR) and are representative of at least two independent experiments.

Immunoprecipitation—3T3-L1 cells were differentiated for 0, 2 or 4 days. Immunoprecipitation was performed as previously described by Anderson et al. (2017) Briefly, mitochondrial pellets were isolated and homogenized in a cold lysis buffer (50 mM Tris HCl, pH 8.0, 150 mM NaCl, 0.5% Triton X-100, 2 mM EDTA, 40 mM NaF and

protease inhibitor cocktails). Immunoprecipitation of MCCC was performed overnight at 4°C (Santa Cruz, sc-271427), bound to A/G agarose beads and washed 3 times and run by western blotting.

RNA isolation and RT-PCR—RNA was extracted with the Quick-RNA MiniPrep kit (Zymo Research) directly from adherent cells. cDNA was synthesized from 1 μg of RNA using the iScript cDNA synthesis kit (Bio-Rad). Real-time qPCR was performed on a Light Cycler 480 (Roche) using PerfeCta SYBR Green Fast Mix (Quanta BioSciences). Primers sequences are listed in supporting document Table S1.

Metabolite profiling—Prior to experiments, cells were differentiated in a time course as indicated. Samples were plated in quadruplicate for metabolite extraction and in quadruplicate for cell count normalization. For metabolite extraction cells were washed once with ice-cold PBS, and polar metabolites were extracted directly on the dish using 1 mL ice-cold 80% methanol.

Cells were seeded and differentiated as for whole cell metabolite extraction. Media without cells was used to determine if metabolites were taken up or secreted.

Metabolites were analyzed on two distinct methods of hydrophilic interaction liquid chromatography coupled to mass spectrometry (HILIC-MS). In one method, electrospray ionization was tailored to negative-ion mode, and in the second method to positive-ion mode. For negative-ion mode, analytes were eluted in Buffer A (20 mM Ammonium Acetate, 20 mM Ammonium Hydroxide) and Buffer B (10 mM Ammonium Hydroxide in 75:25 Acetonitrile:Methanol). Samples were run on a HILIC silica (3 um, 2.1 × 150 mm) column (Waters) with a binary flow rate of 0.4mL/min for 10 minutes on linear gradient (95% Buffer B to 0% Buffer B) followed by 2 minutes with (0% Buffer B) and ending with a 2 minute linear gradient (0% Buffer B to 95% Buffer B) and holding (95% Buffer B) for 13 minutes. For positive-ion mode, samples were dried down and reconstituted in a 20:70:10: acetonitrile:MeOH:water mixture. The buffers were: Buffer A (10 mM Ammonium Formate, 0.1% formic acid in water) and Buffer B (Acetonitrile, 0.1% formic acid). Samples were run on a HILIC silica (3 um, 2.1 × 150 mm) column (Waters) with a binary flow rate of 0.25mL/min for 10 minutes on linear gradient (95% Buffer B to 40% Buffer B) followed by 4.5 minutes with (40% Buffer B) and ending with a 2 minute linear gradient (40% Buffer B to 95% Buffer B) and holding (95% Buffer B) for 13 minutes. For both ion-modes, a Q Exactive hybrid quadrupole orbitrap mass spectrometer (Thermo Fisher Scientific) with a full-scan analysis over 70–800 m/z and high resolution (70,000) was used for mass detection. A targeted-method developed for 176 compounds (118 on positive and 58 on negative) was used to identify metabolites. A master mix of reference standards for metabolites in the targeted method were run immediately prior to each set of samples, such that their retention times were associated with peaks in the unknown samples run over that same column. Peaks were integrated in Tracefinder 3.3. Metabolite levels were normalized to cell number from a parallel plate.

The extract was separated by using an iHILIC column (5 μm, 150 × 2.1 mm I.D., HILICON) coupled to a Thermo Scientific SII UPLC system. The iHILIC column was used with the

following buffers and linear gradient: A = water with 20 mM ammonium carbonate with 0.1% ammonium hydroxide, B = acetonitrile; 95% to 50% B from 0 – 15min, 50% to 20% B from 15–20min; flow rate 150 μL/min. Mass spectrometry detection was carried out on a Q Extractive HF-X orbitrap mass spectrometer with an HESI source operated in negative mode.

Leucine tracing—For leucine tracing experiments, cells were incubated in leucine free media supplemented with 10mM L-Leucine-$^{13}C_6$ (Sigma #605239) for 8 hours. Metabolites were isolated in 80% HPLC-grade methanol. An Agilent 6470 Triple Quadrupole mass spectrometer was used for mass detection. The untreated control was used to determine the natural abundance of ^{13}C metabolites. The incorporation was measured as:

$$\% = (Ion\ count(M+2))/(Ion\ count(M+2) + Ion\ count) \times 100$$

MCCC1 activity assay—Mitochondria were isolated from 3T3-L1 cells after washing cells with ice-cold PBS and homogenizing 20 times using a glass-teflon homogenizer in 500 μL STE buffer (0.25 M sucrose, 10 mM Tris-HCl, pH 8, 1 mM EDTA and protease inhibitor tablet). The homogenates were centrifuged at 700 g for 10 min at 4°C and the resulting mitochondria-containing supernatant was centrifuged at 7000 g for 10 min at 4°C pelleting mitochondria. Mitochondrial pellets were resuspended in 100 μL permeabilization buffer (105 mM K-MES, pH 7.1, 30 mM KCl, 10 mM KH_2PO_4, 5 mM $MgCl_2$, 0.5 mg/mL BSA, 50mg/ml digitonin) and incubated for 5 min. To 10 μL of permeabilized mitochondria we added 100 μL MCCC1 reaction buffer (105 mM K-MES, pH 7.1, 30 mM KCl, 10 mM KH_2PO_4, 5 mM $MgCl_2$, 0.5 mg/mL BSA, 2 mM ATP, 0.1 mM DTT, 0.3 mM methylcrotonyl-CoA and 3 μCi $NaH[^{14}C]O_3$). The reaction was performed for 30 min at 37°C and then stopped with HCl. Unreacted $NaH[^{14}C]O_3$ was evaporated by placing Eppendorf tubes with lids open at 60°C overnight in a fume hood. The remaining product containing production of [^{14}C]3-methylglutaconyl-CoA was resuspended in 500 μL H_2O and analyzed on the scintillation counter. Counts per minute (cpm) were normalized to protein content.

Respiration—Respiration was assessed using the Seahorse XFe-96 Analyzer (Seahorse Bioscience). Cells were differentiated for indicated times prior to measuring respiration. Following this incubation, media was changed to a non-buffered, serum-free Seahorse Media (Seahorse Bioscience, Catalog #102353) supplemented with 5 mM glucose, 2 mM L-glutamine, and 1 mM sodium pyruvate. For ketoisocaproic acid mediated respiration cells were permeabilized in MAS (220 mM mannitol, 70 mM sucrose, 10 mM KH_2PO_4, 5 mM $MgCl_2$, 2 mM HEPES, 1 mM EGTA) medium supplemented with 0.2% (w/v) BSA, 4 mM ADP, 5 mM ketoisocaproic acid, 0.5mM D-malic acid and 2 nM XF Plasma Membrane Permeabilizer, (Seahorse Bioscience). Values were normalized to protein content.

Animal studies—Studies were performed according to protocols approved by the Institutional Animal Care and Use Committee, the Standing Committee on Animals at Harvard. Female mice that were 8–10 weeks old were fed a normal chow diet (PicoLab Diet 5053). Body weight was measured weekly.

Metabolic cage studies—In this experiment a total of 12 female mice (20–22 weeks of age) were placed into the CLAMS. The mice were consecutively exposed to 72 hours of 22°C and 4°C. The 72 hours were divided into 48 hours of acclimation followed by 24 hours of data collection. Body-weights and body compositions, analyzed via echoMRI, were determined before the 22°C and 4°C data collection period. All graphs represent averages per hour per group, and error bars represent SEM.

Bioinformatics—A list of correlated expression transcripts of Sirtuin4 was generated by the Attie Lab Diabetes Database, using search criteria “adipose,” “mlratio,” “200,” and “$p < 0.05$.” This provided a list of the 200 most correlated transcripts of Sirt4 in the selected tissue. To generate the graph data, the correlated Attie Lab data were processed by the DAVID Bioinformatics Database. 135 transcripts were identified with their official gene symbol and grouped related cellular processes with their P value of occurrence and number of included proteins. The pathway selected was the KEGG pathway, which returned 13 processes grouping a total of 35 proteins. Two of these processes, “Carbon Metabolism” and “Metabolic Pathways,” were discarded for being too broad and having little research potential. MATLAB (version R2020b) was used to generate a polar bubble chart. Each data point represents one cellular process, where the size is the number of proteins in that process, and the radial coordinate is the negative logarithm of the P value of each process. Data points are ordered on the graph counterclockwise by −log P and appear in the same order on the legend. Angles of data points are arbitrary and were assigned to space the data adequately.

QUANTIFICATION AND STATISTICAL ANALYSIS

Details regarding the specific statistical tests, definition of center, and number of replicates (n), can be found for each experiment in the figure legends. GraphPad Prism and excel were used for all quantifications and statistical analyses. Statistical significance between groups was determined using the unpaired Student’s t test (unless otherwise noted). Significance is reported as follows: $*p \leq 0.05$, $**p \leq 0.01$, $***p \leq 0.001$, and $****p \leq 0.0001$. All experiments were performed at least two to three times. The replicates are biological.

Supplementary Material

Refer to Web version on PubMed Central for supplementary material.

ACKNOWLEDGMENTS

We thank Ilaria Elia, Jiska van Der Reest, and Jefte Drijvers for thoughtful discussion on this manuscript. E.Z. was supported by a postdoctoral fellowship from the American Heart Association (15POST25560077), and M.C.H. is funded by NIH grant from NIDDK (R01DK103295-01A1) and the Glenn Foundation for Medical Research. Microscopy experiments were performed at the Nikon Imaging Center at Harvard Medical School. Metabolic cage studies were performed by the Brigham and Women’s Hospital Metabolic Core. Rodent Histopathology (DF/HCC) core at Harvard Medical School was used for tissue sectioning and H&E staining.

REFERENCES

Anderson KA, Huynh FK, Fisher-Wellman K, Stuart JD, Peterson BS, Douros JD, Wagner GR, Thompson JW, Madsen AS, Green MF, et al. (2017). SIRT4 Is a Lysine Deacylase that Controls Leucine Metabolism and Insulin Secretion. Cell Metab 25, 838–855.e15. [PubMed: 28380376]

Bheda P, Jing H, Wolberger C, and Lin H (2016). The Substrate Specificity of Sirtuins. Annu. Rev. Biochem 85, 405–429. [PubMed: 27088879]

Blanchard PG, Moreira RJ, Castro É, Caron A, Côté M, Andrade ML, Oliveira TE, Ortiz-Silva M, Peixoto AS, Dias FA, et al. (2018). PPARγ is a major regulator of branched-chain amino acid blood levels and catabolism in white and brown adipose tissues. Metabolism 89, 27–38. [PubMed: 30316815]

Feldman JL, Dittenhafer-Reed KE, and Denu JM (2012). Sirtuin catalysis and regulation. J. Biol. Chem 287, 42419–42427. [PubMed: 23086947]

Felig P, Marliss E, and Cahill GF Jr. (1969). Plasma amino acid levels and insulin secretion in obesity. N. Engl. J. Med 281, 811–816. [PubMed: 5809519]

Fernandez S, Viola JM, Torres A, Wallace M, Trefely S, Zhao S, Affronti HC, Gengatharan JM, Guertin DA, Snyder NW, et al. (2019). Adipocyte ACLY Facilitates Dietary Carbohydrate Handling to Maintain Metabolic Homeostasis in Females. Cell Rep 27, 2772–2784.e6. [PubMed: 31141698]

Giblin W, Skinner ME, and Lombard DB (2014). Sirtuins: guardians of mammalian healthspan. Trends Genet 30, 271–286. [PubMed: 24877878]

Green CR, Wallace M, Divakaruni AS, Phillips SA, Murphy AN, Ciaraldi TP, and Metallo CM (2016). Branched-chain amino acid catabolism fuels adipocyte differentiation and lipogenesis. Nat. Chem. Biol 12, 15–21. [PubMed: 26571352]

Gregoire FM, Smas CM, and Sul HS (1998). Understanding adipocyte differentiation. Physiol. Rev 78, 783–809. [PubMed: 9674695]

Haigis MC, Mostoslavsky R, Haigis KM, Fahie K, Christodoulou DC, Murphy AJ, Valenzuela DM, Yancopoulos GD, Karow M, Blander G, et al. (2006). SIRT4 inhibits glutamate dehydrogenase and opposes the effects of calorie restriction in pancreatic beta cells. Cell 126, 941–954. [PubMed: 16959573]

Herman MA, She P, Peroni OD, Lynch CJ, and Kahn BB (2010). Adipose tissue branched chain amino acid (BCAA) metabolism modulates circulating BCAA levels. J. Biol. Chem 285, 11348–11356. [PubMed: 20093359]

Keller MP, Choi Y, Wang P, Davis DB, Rabaglia ME, Oler AT, Stapleton DS, Argmann C, Schueler KL, Edwards S, et al. (2008). A gene expression network model of type 2 diabetes links cell cycle regulation in islets with diabetes susceptibility. Genome Res 18, 706–716. [PubMed: 18347327]

Kusminski CM, Holland WL, Sun K, Park J, Spurgin SB, Lin Y, Askew GR, Simcox JA, McClain DA, Li C, and Scherer PE (2012). MitoNEET-driven alterations in adipocyte mitochondrial activity reveal a crucial adaptive process that preserves insulin sensitivity in obesity. Nat. Med 18, 1539–1549. [PubMed: 22961109]

Laurent G, de Boer VC, Finley LW, Sweeney M, Lu H, Schug TT, Cen Y, Jeong SM, Li X, Sauve AA, and Haigis MC (2013a). SIRT4 represses peroxisome proliferator-activated receptor α activity to suppress hepatic fat oxidation. Mol. Cell. Biol 33, 4552–4561. [PubMed: 24043310]

Laurent G, German NJ, Saha AK, de Boer VC, Davies M, Koves TR, Dephoure N, Fischer F, Boanca G, Vaitheesvaran B, et al. (2013b). SIRT4 coordinates the balance between lipid synthesis and catabolism by repressing malonyl CoA decarboxylase. Mol. Cell 50, 686–698. [PubMed: 23746352]

Mathias RA, Greco TM, Oberstein A, Budayeva HG, Chakrabarti R, Rowland EA, Kang Y, Shenk T, and Cristea IM (2014). Sirtuin 4 is a lipoamidase regulating pyruvate dehydrogenase complex activity. Cell 159, 1615–1625. [PubMed: 25525879]

Neinast MD, Jang C, Hui S, Murashige DS, Chu Q, Morscher RJ, Li X, Zhan L, White E, Anthony TG, et al. (2019). Quantitative Analysis of the Whole-Body Metabolic Fate of Branched-Chain Amino Acids. Cell Metab 29, 417–429.e4. [PubMed: 30449684]

Newgard CB, An J, Bain JR, Muehlbauer MJ, Stevens RD, Lien LF, Haqq AM, Shah SH, Arlotto M, Slentz CA, et al. (2009). A branched-chain amino acid-related metabolic signature that differentiates obese and lean humans and contributes to insulin resistance. Cell Metab 9, 311–326. [PubMed: 19356713]

Pietiläinen KH, Naukkarinen J, Rissanen A, Saharinen J, Ellonen P, Keränen H, Suomalainen A, Götz A, Suortti T, Yki-Järvinen H, et al. (2008). Global transcript profiles of fat in monozygotic twins discordant for BMI: pathways behind acquired obesity. PLoS Med 5, e51. [PubMed: 18336063]

Rosen ED (2005). The transcriptional basis of adipocyte development. Prostaglandins Leukot. Essent. Fatty Acids 73, 31–34. [PubMed: 15936931]

Trefely S, and Wellen KE (2018). Metabolite regulates differentiation. Science 360, 603–604. [PubMed: 29748271]

van de Ven RAH, Santos D, and Haigis MC (2017). Mitochondrial Sirtuins and Molecular Mechanisms of Aging. Trends Mol. Med 23, 320–331. [PubMed: 28285806]

Wirth M, Karaca S, Wenzel D, Ho L, Tishkoff D, Lombard DB, Verdin E, Urlaub H, Jedrusik-Bode M, and Fischle W (2013). Mitochondrial SIRT4-type proteins in Caenorhabditis elegans and mammals interact with pyruvate carboxylase and other acetylated biotin-dependent carboxylases. Mitochondrion 13, 705–720. [PubMed: 23438705]

Wu Z, Rosen ED, Brun R, Hauser S, Adelmant G, Troy AE, McKeon C, Darlington GJ, and Spiegelman BM (1999). Cross-regulation of C/EBP alpha and PPAR gamma controls the transcriptional pathway of adipogenesis and insulin sensitivity. Mol. Cell 3, 151–158. [PubMed: 10078198]

Yang W, Nagasawa K, Münch C, Xu Y, Satterstrom K, Jeong S, Hayes SD, Jedrychowski MP, Vyas FS, Zaganjor E, et al. (2016). Mitochondrial Sirtuin Network Reveals Dynamic SIRT3-Dependent Deacetylation in Response to Membrane Depolarization. Cell 167, 985–1000.e21. [PubMed: 27881304]

Yoneshiro T, Wang Q, Tajima K, Matsushita M, Maki H, Igarashi K, Dai Z, White PJ, McGarrah RW, Ilkayeva OR, et al. (2019). BCAA catabolism in brown fat controls energy homeostasis through SLC25A44. Nature 572, 614–619. [PubMed: 31435015]

Zaganjor E, Vyas S, and Haigis MC (2017). SIRT4 Is a Regulator of Insulin Secretion. Cell Chem. Biol 24, 656–658. [PubMed: 28644956]

Highlights

- Branched-chain amino acid (BCAA) oxidation drives early adipocyte differentiation
- BCAA catabolism precedes PPARγ transcriptional activity
- The mitochondrial sirtuin SIRT4 promotes BCAA catabolism and adipogenesis
- The SIRT4-BCAA catabolism axis is downregulated in the adipose tissue of diabetic mice

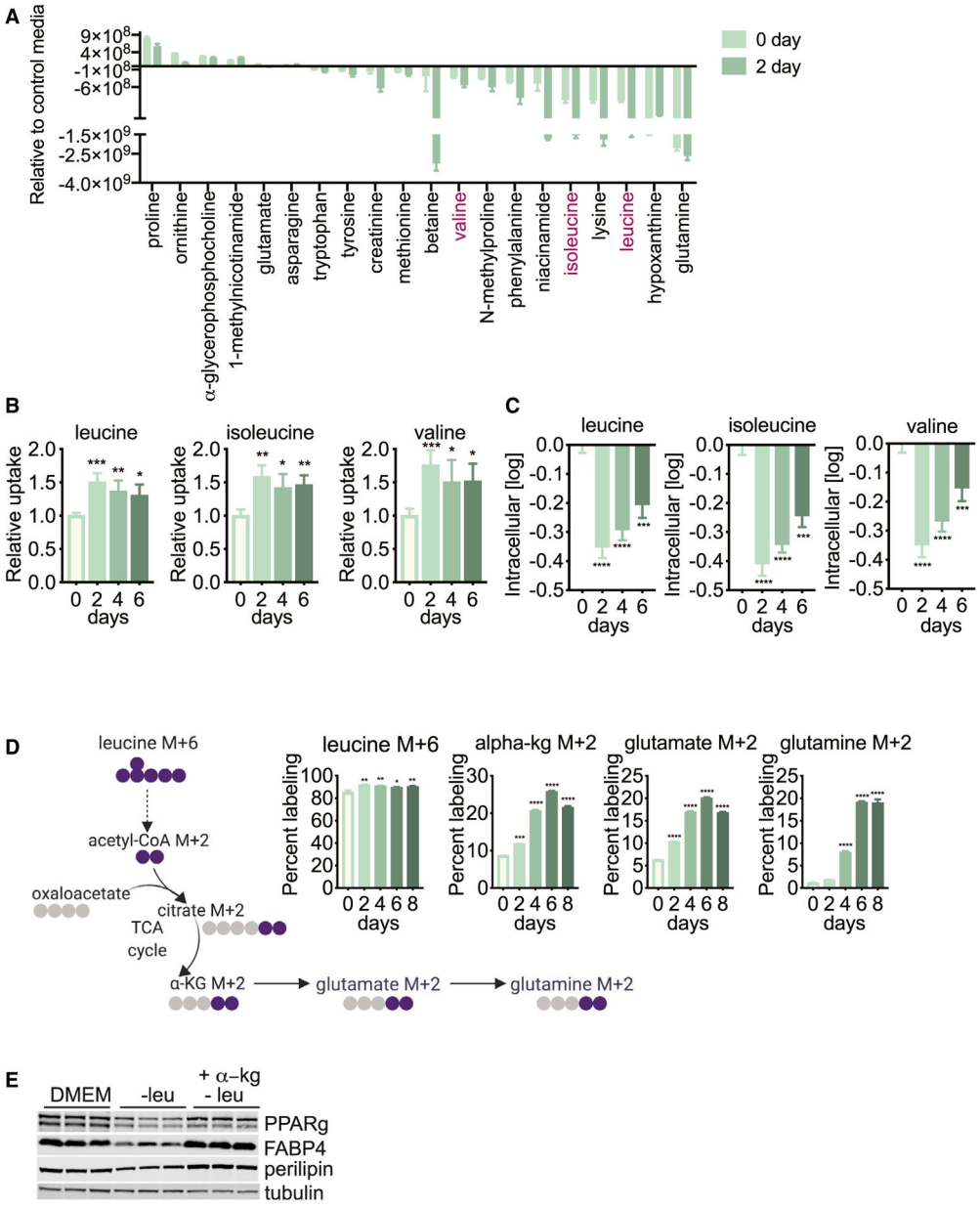

Figure 1. BCAA catabolism is induced in early adipogenesis

(A) Metabolites that are most taken up or secreted by 3T3-L1 cells and are significantly altered after 2 days of differentiation; they were normalized to control media without cells. Data shown are from 4 biological replicates.

(B) Leucine, isoleucine, and valine uptake during a time course of 3T3-L1 differentiation relative to undifferentiated state. Data shown are from 4 biological replicates.

(C) Intracellular abundance of leucine, isoleucine, and valine measured from 3T3-L1 cells differentiated from 0 to 6 days and normalized to undifferentiated cells. Data shown are from 4 biological replicates.

(D) Isotope abundance of ^{13}C-leucine-derived metabolites during the time course of 3T3-L1 differentiation. Data shown are from 3 biological replicates.

(E) Differentiation markers perilipin, FABP4, and PPARγ were analyzed by western blot after 8 days of differentiation in DMEM or leucine-free DMEM with or without supplementation of 10 mM dimethyl-α-ketoglutarate (α-kg). Presented replicates are biological. Data are representative of 3 independent experiments. Error bars indicate mean ± SEM; *$p \leq 0.05$, **$p \leq 0.01$, and ***$p \leq 0.001$.

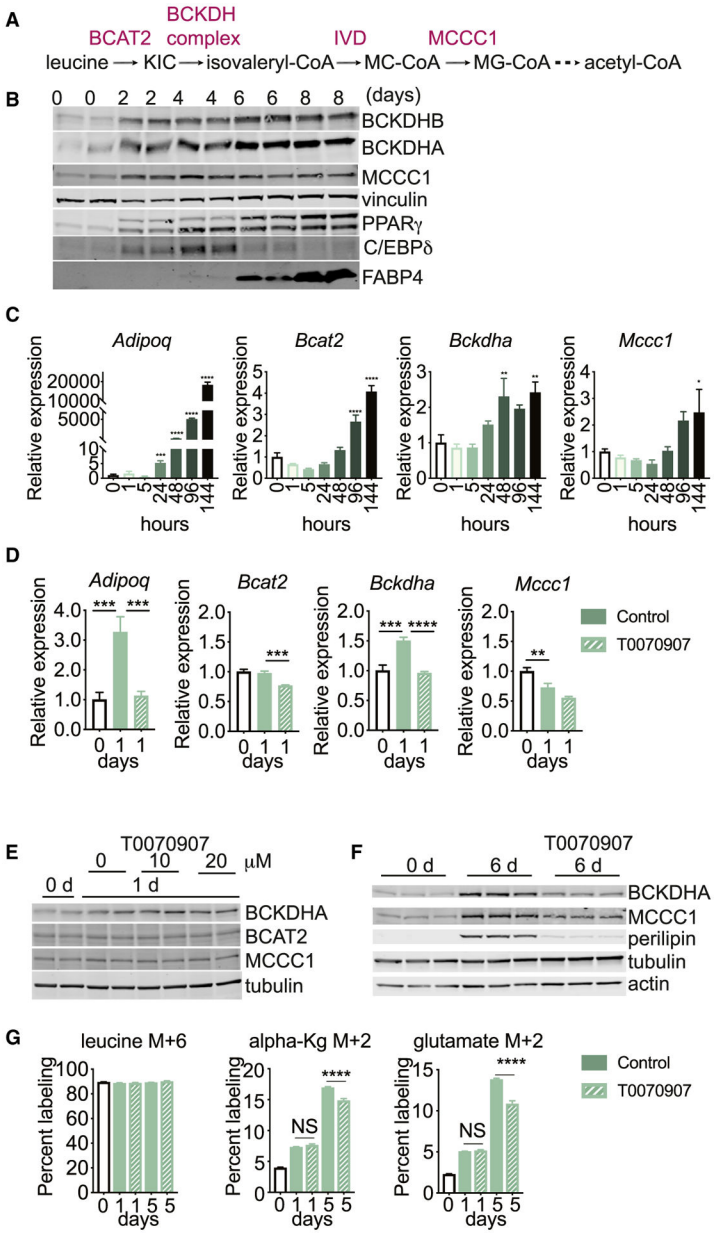

Figure 2. BCCA catabolism during early adipogenesis is not dependent on PPARγ

(A) BCAA pathway schematic.

(B) Protein expression of BCAA enzymes analyzed by western blot from 3T3-L1 cells undifferentiated or differentiated in a time course as indicated. PPARγ, c/EBPδ, and FABP4 used as markers of distinct differentiation stages. Biological duplicates presented.

(C) qPCR analysis of *Adipoq*, *Bcat2*, *Bckdha*, and *Mccc1* gene expression after a differentiation time course, as indicated. Three biological replicates are presented.

(D) qPCR analysis of *Adipoq*, *Bcat2*, *Bckdha*, and *Mccc1* gene expression after a 1-day treatment with 20 μM T0070907. Three biological replicates were used.

(E) Expression of BCAA enzymes after a 1-day treatment with or without 10 μM or 20 μM T0070907, analyzed by western blot. Undifferentiated samples (0 d) were used as controls. Biological duplicates are presented.

(F) Expression of BCAA enzymes after a 6-day treatment with or without 10 μM T0070907, analyzed by western blot. Undifferentiated samples (0 d) were used as controls. Biological triplicates are presented.

(G) Isotope abundance of ^{13}C-leucine-derived metabolites in 3T3-L1 cells differentiated for 1 or 5 days treated with or without 20 μM T0070907. Undifferentiated samples (day 0) were used as controls. Data shown are from 3 biological replicates.

Error bars indicate mean ± SEM; *$p \leq 0.05$, **$p \leq 0.01$, and ***$p \leq 0.001$. All data are representative of 2–3 independent experiments.

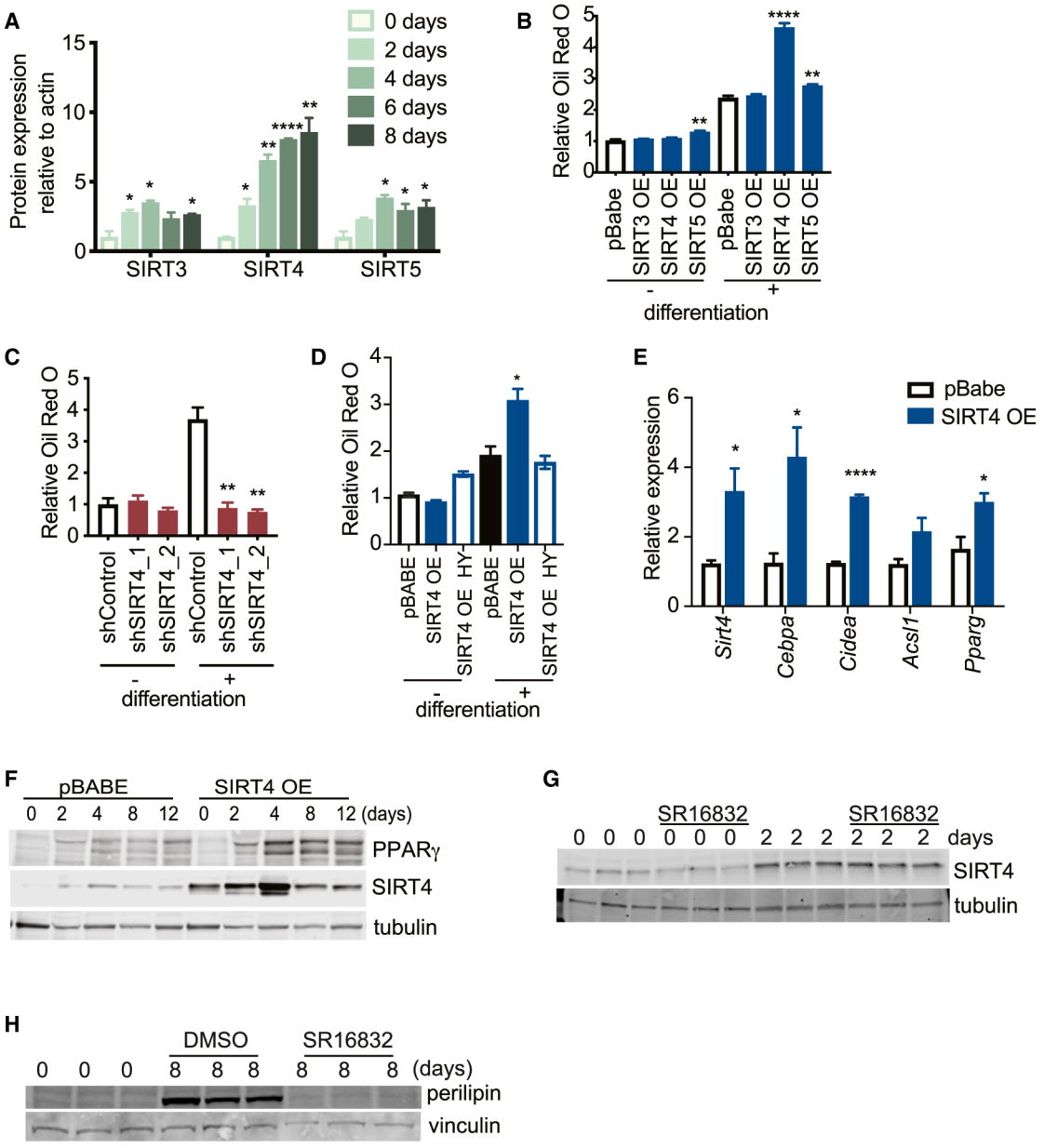

Figure 3. SIRT4 promotes adipogenesis and PPARγ

(A) Quantification of western blot band intensity for SIRT3, SIRT4, and SIRT5 from Figure S3A normalized to actin. Biological duplicates were used.

(B) Quantification of oil red O normalized to crystal violet in 3T3-L1 cells overexpressing (OE) pbabe-HA-SIRT3, pbabe-HA-SIRT4, and pbabe-HA-SIRT5 in undifferentiated and differentiated states. Six biological replicates were plotted.

(C) Quantification of oil red O normalized to crystal violet in shControl or shSIRT4 3T3-L1 cells in undifferentiated and differentiated states. Biological triplicates were plotted.

(D) Quantification of oil red O normalized to crystal violet in 3T3-L1 overexpressing WT HA-SIRT4 or mutant HA-H162Y SIRT4 (SIRT4 HY) in undifferentiated and differentiated states. Data represent biological duplicates.

(E) qPCR gene expression analysis of *Sirt4*, *CEBPα*, *Cidea*, *Acsl1*, and *PPARγ* in control 3T3-L1 or SIRT4-overexpressing 3T3-L1 cells after 8 days of differentiation. Values represent mean ± SD, n = 3.
(F) PPARγ, SIRT4, and tubulin were detected by immunoblotting in control or SIRT4-overexpressing 3T3-L1 cells differentiated 0, 2, 4, 8, and 12 days.
(G) Western blot analysis of SIRT4 and tubulin in 3T3-L1 cells differentiated for 0 or 2 days with or without 10 μM SR16832. Biological triplicates are presented.
(H) Western blot analysis of perilipin and vinculin in 3T3-L1 cells differentiated for 0 or 8 days with or without 10 μM SR16832. Biological triplicates are presented. All data are representative of 2–3 independent experiments.

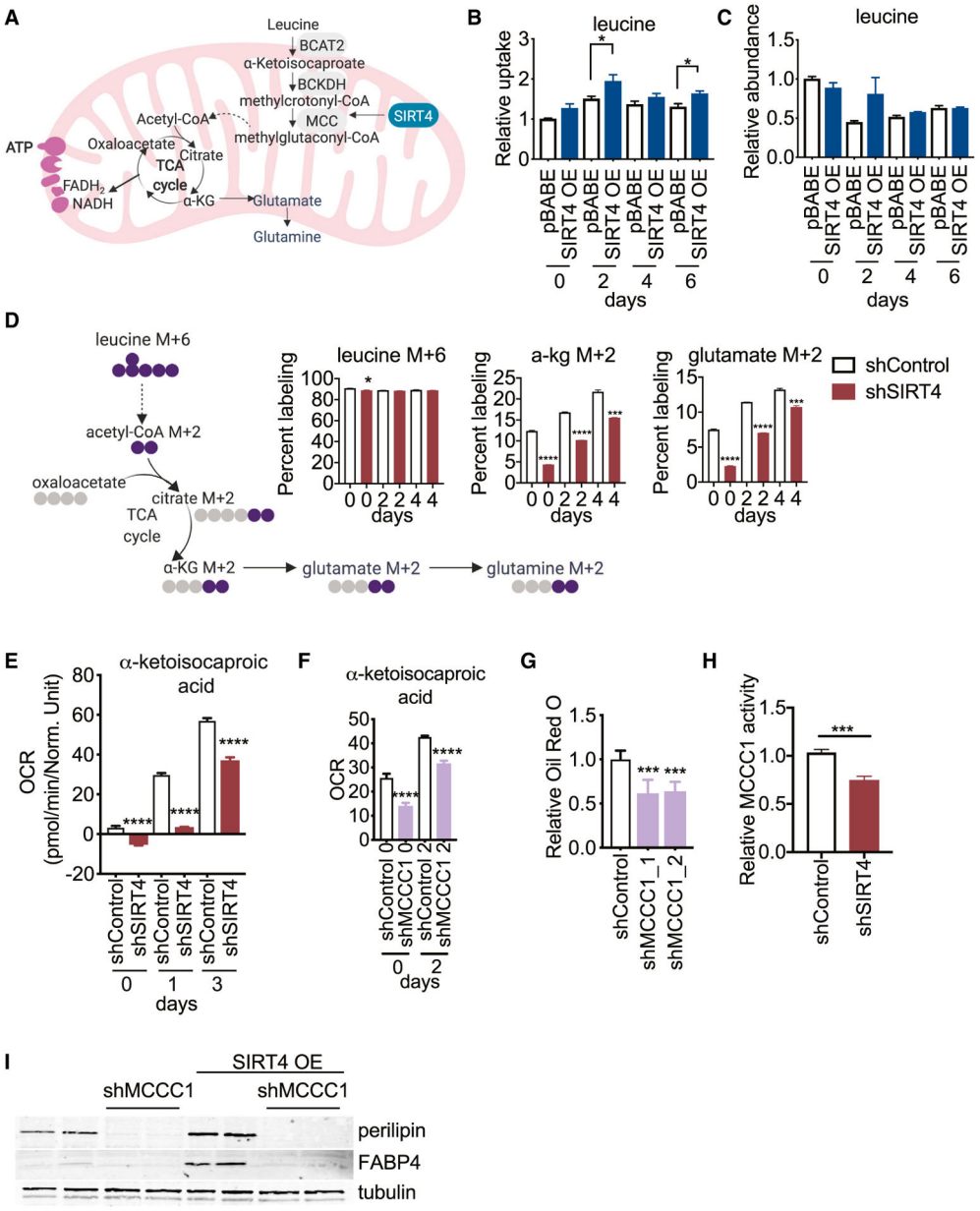

Figure 4. SIRT4 promotes BCAA catabolism

(A) Model for SIRT4 regulation of BCAA catabolism.

(B) Relative leucine uptake from control and SIRT4-overexpressing 3T3-L1 cells differentiated from 0 to 6 days, normalized to control media without cells. Data depict biological quadruplicates.

(C) Intracellular abundance of leucine from control and SIRT4-overexpressing 3T3-L1 cells differentiated from 0 to 6 days. Data depict biological quadruplicates.

(D) Isotope abundance of ^{13}C-leucine-derived metabolites in control or shSIRT4 3T3-L1 cells differentiated for 0, 2, and 4 days. Data represent biological triplicates.

(E) α-Ketoisocaproic-acid-mediated oxygen consumption rate (OCR) in permeabilized control or shSIRT4 3T3-L1 cells differentiated for 0, 1, and 3 days.

(F) α-Ketoisocaproic-acid-mediated OCR in permeabilized shControl or shMCCC1 3T3-L1 cells differentiated for 0 and 2 days.
(G) Quantification of relative oil red O in shControl or shMCCC1 3T3-L1 cells differentiated for 8 days. Six biological replicates were used.
(H) MCCC1 activity in shControl or shSIRT4 3T3-L1 cells differentiated for 2 days. Four biological replicates were used.
(I) Western blot analysis of perilipin and FABP4 in 3T3-L1 cells differentiated 6 days overexpressing SIRT4 or control vector and shMCCC1 or control plasmid. Biological duplicates are presented.
Error bars indicate mean ± SEM; *$p \leq 0.05$, **$p \leq 0.01$, and ***$p \leq 0.001$. All data are representative of 2–3 independent experiments.

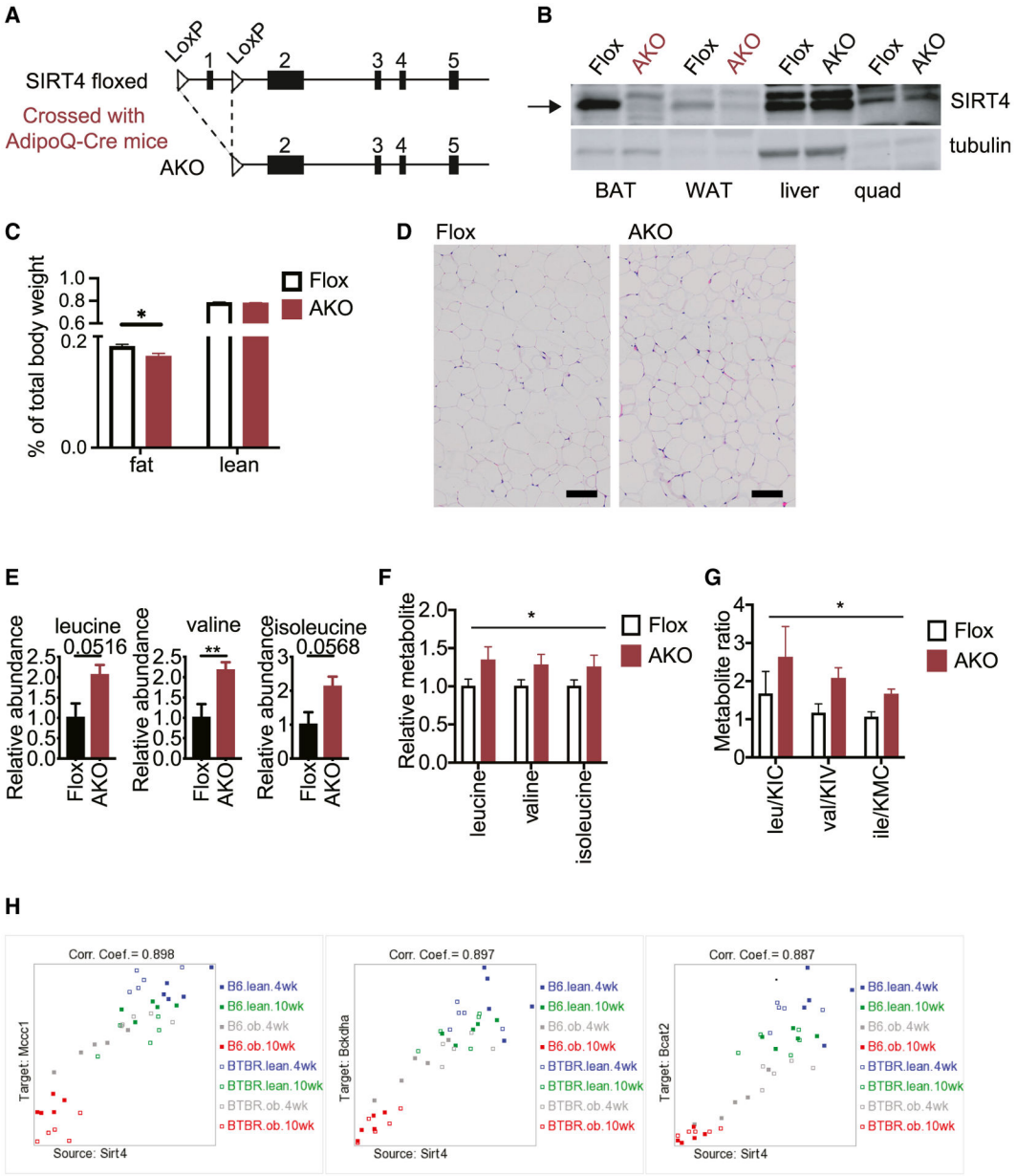

Figure 5. Loss of SIRT4 in the adipose tissue in vivo results in decreased BCAA catabolism

(A) Schematic of construction of SIRT4 flox allele (Flox) crossed with AdipoqCre to generate adipose-tissue-specific SIRT4 knockdown (AKO) mice.

(B) Western blot analysis of SIRT4 and tubulin from mouse tissues (brown adipose tissue [BAT], white adipose tissue [WAT], liver, and quadriceps muscle [quad]), from Flox and AKO mice.

(C) Lean and fat mass from Flox and AKO mice were measured by echoMRI (n = 12 of each genotype).

(D) Representative hematoxylin and eosin (H&E)stainingof gonadal white adipose tissue from Flox and AKO mice fed standard chow diet; scale bars indicate100 μm.

(E) Relative BCAA levels (leucine, valine, iand soleucine) from gonadal white adipose tissue of Flox and AKO mice fed standard chow diet, n = 4.
(F) Relative BCAA levels (leucine, valine, and isoleucine) in the plasma of Flox and AKO mice fed standard chow diet, n = 4. Two-way ANOVA statistical analysis.
(G) Ratio of BCAA/ketoacids normalized to Flox control samples from metabolites presented in Figures 5F and S5E. Two-way ANOVA statistical analysis, n = 4.
(H) Correlation coefficients for the top genes (*Mccc1*, *Bckdha*, and *Bcat2*) that correlated with SIRT4 expression in adipose tissue of control and ob/ob mice.
Error bars indicate mean ± SEM; *p ≤ 0.05, **p ≤ 0.01, and ***p ≤ 0.001.

KEY RESOURCES TABLE

REAGENT or RESOURCE	SOURCE	IDENTIFIER
Antibodies		
Rabbit monoclonal PPARγ	Cell signaling	Cat# 2443S; RRID:AB_823598
Rabbit monoclonal perilipin	Cell signaling	Cat# 9349; RRID:AB_10829911
Rabbit monoclonal FABP4	Cell signaling	Cat# 3544T; RRID:AB_2278257
Mouse monoclonal tubulin	Novus Biologicals	Cat# NB100-690; RRID:AB_521686
Rabbit polyclonal BCKDHA	LSBio	Cat#LS-C411335
Rabbit polyclonal BCKDHB	Proteintech	Cat#13685-1-AP; RRID:AB_2877972
Mouse monoclonal MCCA	Santa Cruz	Cat# sc-271427; RRID:AB_10658968
Mouse monoclonal Vinculin	Santa Cruz	Cat#sc-25336; RRID:AB_628438
Rabbit polyclonal pS6	Cell signaling	Cat# 5364; RRID:AB_10694233
Rabbit ribosomal S6	Novus Biologicals	Cat#NN100-1595
Rabbit SIRT4	Haigis et al., 2006 and Invitrogen	Cat# 96727; RRID:AB_2808529
Rabbit monoclonal SirT3	Cell signaling	Cat# 5490S; RRID:AB_10828246
Rabbit monoclonal SirT5	Cell signaling	Cat# 8782S; RRID:AB_2716763
Rabbit methylglutaryl-lysine	Millipore	Cat#ABS2120
Rabbit polyclonal C/EBPδ	Cell signaling	Cat#2318T; RRID:AB_2078194
Mouse monoclonal HA	Cell signaling	Cat#2367S; RRID:AB_10691311
Mouse Monoclonal GAPDH	Novus Biologicals	Cat#NB300-221; RRID:AB_10077627
Rabbit polyclonal actin	Sigma-Aldrich	Cat# A2066; RRID:AB_476693
Alexa Fluor 546 Goat Anti-Rabbit IgG (H+L)	Life-Tech	Cat# A-11035; RRID:AB_143051
Alexa Fluor 488 Goat Anti-Mouse IgG (H+L)	Life-Tech	Cat# A-11029; RRID:AB_138404
Chemicals, peptides, and recombinant proteins		
SR 16832	Tocris	Cat# 6383
T0070907	Cayman Chemicals	Cat#313516-66-4
α-ketoisocaproic acid	Sigma	Cat# 68255
Dulbecco Modified Eagle Medium	Life Technologies	Cat# 11995
penicillin-streptomycin	Life Technologies	Cat# 15140-122
Puromycin	InvivoGen	Cat# ant-pr-1
L-leucine-$^{13}C_6$	Sigma	Cat# 605239
Beta-methylcrotonyl coenzyme A lithium salt	Sigma	Cat# M3013
Insulin	Sigma	Cat# I0516
1-isobutyl-1-methylxanthine	Sigma	Cat# I7018
Dexamethasone	Sigma	Cat# D4902
Experimental models: Cell lines		
3T3-L1	ATCC	CL-173
NIH 3T3	ATCC	CRL-1658
Experimental models: Organisms/strains		
C57BL/6	Jackson Labs	Cat# 000664
Oligonucleotides		

REAGENT or RESOURCE	SOURCE	IDENTIFIER
qPCR primers: see Table S1	This paper	N/A
shRNA primers: see Table S2	This paper	N/A
Recombinant DNA		
Plasmid: pBabe-hSIRT5	Yang et al., 2016	N/A
Plasmid: pBabe-hSIRT3	Yang et al., 2016	N/A
Plasmid: pBabe-mSIRT4, pBabe-mSIRT4H162Y	Laurent et al., 2013b	N/A
Software and algorithms		
Attie Lab Diabetes Database	http://diabetes.wisc.edu/search.php	N/A
GraphPad Prism 7.0	GraphPad Software	N/A
Image Studio 4.0	Odyssey CLx Software	N/A
MetaboAnalyst 4.0	https://www.metaboanalyst.ca	N/A